Data from a pilot plant experiment for the processing of a complex tin skarn ore – 19.11.2018

1. Introduction to the data set

This data set derives from a pilot plant campaign for the beneficiation of a complex tin bearing skarn ore, including different separation and classification steps. The aim of the pilot plant test work was to prove a flowsheet that had been developed based on detailed geometallurgical analysis and results from the research projects AFK (Aufbereitung feinkörniger Komplexerze, BMBF grant number 033R128) and FAME (European Union grant 641650) to produce a cassiterite concentrate for tin production, and further preconcentrates for iron, zinc, copper, indium, and arsenic. The tin mineralization is partially well localized in cassiterite, but also partially finely disseminated and thus unrecoverable as minor components in other minerals. The iron is located in magnetic and nonmagnetic iron oxides sometimes intergrown with cassiterite. Therefore, iron concentrates are recovered at larger grain sizes but need a further tin recovery step not implemented in the reported experiment. The other elements are mainly deported in sulfides, which are bulk recovered in a flotation step. A subsequent selective flotation is needed to recover them individually. This selective flotation is, however, not part of the reported experiment. The two tin concentrates recovered from the shaking table should be considered as preconcentrates, that can be enriched further e.g. through multi stage gravity separation.

The motivation for this data set is to provide a consistent basis for the application of new particle based geometallurgical methods enabled by automated mineralogy (e.g. Buchmann et al. 2018; Schach et al. 2019; Buchmann et al. 2020; Pereira et al. 2020).

In addition, it should also allow for the comparison and evaluation of different analytical methods, which were used during the pilot plant experiments to generate a validated data set for the whole plant and to correlate different result from various methods. This is the basis for further investigations enabling the application of various analyzing methods in a synergetic way. Those synergies can help in future to compensate drawbacks of certain methods by an adequate combination of multiple approaches.

This repository includes raw data and processed data from November 19, 2018. The following data is included:

- X-ray fluorescence spectroscopy (XRF)
- X-ray diffraction (XRD)
- Automated Mineralogy (MLA)
- The balanced mass flows and element/mineral grades for the XRF- and the MLA data
- External certified analysis including different inductive coupled plasma (ICP) and XRF methods from ALS
- R scripts for the mass balance

The flow sheet of the Tellerhäuser pilot plant can be found in Appendix 1 and a list of the installed machinery and used operation parameters is presented in Appendix 2.

2. Tellerhäuser Pilot Plant

The Tellerhäuser pilot plant, which operated in November 2018, represents a collaboration of the nationally funded project consortium AFK, the European Union funded project consortium FAME and the junior mining company Saxore Bergbau GmbH with the aim to demonstrate that the economic beneficiation of the complex Tellerhäuser deposit, containing considerable amounts of Sn, Zn and In is feasible. The plant was operated in a quasi-steady state on the 19th and 28th of November 2018, allowing for sampling and evaluation.

3. Sampling

Two different types of samples were taken in the pilot plant: "incremental" samples to determine the volume and mass streams and "cumulative" samples to obtain average chemical and mineralogical information over a whole run of the pilot test. For preparation of the various analyses the samples were dewatered with vacuum filtration and dried in an oven over night.

4. Sample Analysis

Samples were characterized using scanning electron microscopy-energy dispersive X-ray spectroscopy (SEM-EDS)-based image analysis (*aka* automated mineralogy), X-ray powder diffraction (XRD), and X-ray fluorescence analysis (XRF).

4.1 XRF analysis

Samples for XRF were milled to <63μm where necessary (ring mill using agate mortars to avoid magnetic separation in the mill) and dried at 105 °C over night. 10 g of sample material was thoroughly mixed with 2g of wax (CEREOX®) and pressed into pellets of 40mm diameter. Measurements were done using a PANalytical Axios^max minerals and data were evaluated using PANalytical's OMNIAN software package which was precalibrated with special focus on Sn.

Although this method does not provide the most accurate approach, it nevertheless ensured constant and reproducible sample preparation and measurement conditions. It is therefore assumed that the data are comparable at least during the experiment.

4.2 XRD analysis

XRD samples for analysis were pre-milled carefully in a ring mill (Retsch RS200, using agate grinding media) to achieve a grain size of <400μm. The material was then further wet-milled by of use of a McCrone mill (Retsch, zirconium oxide grinding media, in ethanol). After de-agglomeration of the dried samples, they were prepared into 27mm sample holders using the back loading technique. They were then measured using a PANalytical Empyrean X-ray diffractometer, which is equipped with a Co-tube (with primary Fe-filter) operated at 35 kV and 35mA, PIXcel 3D medipix 1x1 area detector. Irradiated area was kept constant using an automatic divergence slit at 15x12mm. Measured range included 5-80° 2theta with a step size of 0.013° 2 theta, total measurement time was 2h30min. Data were evaluated using the pdf4+ 2018 database (ICDD) and the Highscore Software package of pdf4+ PANalytical as well as the BGMN/Profex software package Doebelin and Kleeberg 2015.

4.3 Automated Mineralogy (MLA)

Nineteen samples from the processing steps S1-S19 (see Appendix 1) were selected for analysis with scanning electron microscopy-energy dispersive X-ray spectroscopy (SEM-

EDS)-based image analysis (aka (a.k.a. Automated Mineralogy; see Chaper 5.3). The samples were homogenized and split into several subsamples. 30 mm grain mounts were prepared by mixing 5 g aliquots with the same volume of graphite and epoxy resin. While the epoxy cures, a gravity-related settlement effect may be expected due to the discrepancy in densities between cassiterite (ρ = 6.99) and silicates minerals, such as quartz (ρ = 2.65). To prevent bias caused by settling, the grain mounts were cut into vertical slices (B-sections) and prepared as suggested by Heinig et al. 2015. Two separate grain mounts were prepared for S3 and S5 in order to maintain representativeness despite visually coarse grain sizes.

Automated mineralogy (Fandrich et al. 2007; Gu 2003) supplies quantitative mineralogical and textural data that is extracted offline from particle maps. It identifies minerals and calculates information such as modal mineralogy, bulk geochemistry, and mineral associations of the analysed sample as a function of the density, mineral chemistry and the measured surface. For the acquisition of this data set, analyses were performed on a Mineral Liberation Analyzer (MLA) equipped with an FEI Quanta 650 F field emission SEM (FE-SEM) with two Bruker Quantax X-Flash 5030 energy-dispersive X-ray (EDX) detectors. MLA grain-based X-ray mapping (GXMAP) method was selected as the measurement mode for the analysed ore. The discrimination of the minerals by their greyscale (BSE mode), with a closely spaced grid of X-ray points (X-ray mapping) ensures that minerals are reliably identified (Fandrich et al. 2007). Data processing was done applying the modified approach for automated mineralogy (Kern et al. 2018) on the software package MLA Suite 3.1.4.686 including the tools *MLA Image Processing*, *MLA Mineral Reference Editor* and *MLA Dataview*. SEM and MLA operating conditions are listed in Table X. Particle agglomerates were manually deleted from the data set when necessary.

Table 1: SEM and MLA operating conditions for thin sections and grain mounts; HFW = horizontal field width;

SEM settings	Grain mounts	MLA settings	Grain mounts
Acceleration voltage (kV)	25	Pixel size μm	1
Probe current (nA)	10	Resolution (pixels)	1000 x 1000
Spot size	5.60	Step size (pixels)	6 x 6
HFW	1000	Acquisition time (ms)	5
Brightness	93.7	BSE trigger	24 - 255
Contrast	18.5	Minimum particle size (pixels)	4
BSE calibration (Au)	244	Minimum grain size (pixels)	4

Several authors have shown that the distinction of iron oxide minerals (hematite and magnetite) is possible with methods of automated mineralogy in certain cases (e.g. Figueroa et al. 2012; Grant et al. 2018). Following the proposed procedures, we attempted to discriminate the two minerals with the BSE calibration on Cu instead of Au and an acceleration voltage of 15kV in order to achieve higher resolution at relevant grey values. Figure X pictures a BSE Histogram of a typical result from one sample showing a weak bimodal distribution and a significant overlap between the two minerals (The hematite and magnetite peaks are estimated to lie around 198 and 210, respectively). According to an XRD analysis from the same sample, the hematite/magnetite ratio in this sample is roughly 50/50. We made three observations that can explain the strong overlap in BSE values of the two iron oxide minerals: (1) EPMA analyses of hematite and magnetite from Hämmerlein show FeO_{Total} contents of both minerals ranging between 95 and 98 wt.%. Minor and trace elements like Sn, Si, Al account for the balance. The amounts of the minor and trace elements vary strongly between single magnetite and hematite grains. We furthermore observed (2) μm-size intergrowths of the two minerals as well as (3) nm-size inclusions of cassiterite within hematite and magnetite (Kern et al. 2019; Figs 8e and 8f, respectively), resulting in mixed BSE pixels. We conclude that an unequivocal distinction of the two minerals in Hämmerlein samples is not possible with MLA.
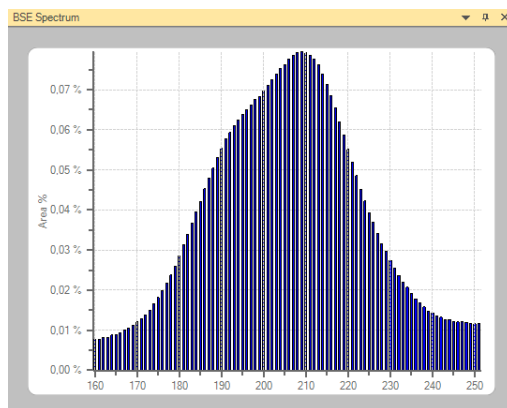
Figure 1. Histogram with BSE overlap of hematite and magnetite showing a bimodal distribution. The instrument was calibrated on Cu (as suggested by Figueroa 2012) for better distinction of the two minerals

4.4   Sample analysis at ALS

Different samples were sent to ALS for comparison and correction of the in-house measurements. Those samples were analysed with different methods which are shortly explained in this chapter. The sample preparation for the respective analysis of all of those samples was done at ALS. The information about the different methods are from the official ALS catalogue (ALS Geochemistry 2020).

ME-ICP06

This method is a multi-element inductive coupled plasma (ICP) optical emission spectroscopy (OES) measurement following a fused based, acid digestion. The loss of ignition is determined from furnace or TGA.

ME-ICP61a

This method uses a four level acid leach to prepare the samples for the ICP-OES measurement.

<u>ME-MS81</u>

The method ME-MS81 includes a lithium borate fusion prior to dissolution and ICP-MS analysis.

<u>ME-XRF15c</u>

This method includes a lithium borate fusion with the addition of strong oxidizing agents to decompose sulphide concentrates. It was mainly used together with the method XRF10 to determine the Sn content in the samples

<u>ME-XRF10</u>

This method is especially used for resistive minerals, which a need a fusion step for complete recovery of the elements.

5. Mass Balancing:

The mass balance for the pilot plant test was done based on the measured mass streams and pressed pellets XRF results. An open source statistic programming language (R), was used to build the mass balance tool. The set of equations for the mass balancing was defined in a way that every single stream was defined by different output streams in the plant. If the stream itself is an output stream, it is only defined by itself. Errors were assigned to the streams and the elemental or mineral compositions were weighted depending on their accuracy and importance. Although sampling in the pilot plant was only done during stable plant conditions, the streams shows significant fluctuations. This can be explained by e.g. a low accuracy of the flowrate measurement especially for the sampling points with high volume streams. For minerals and elements the relative errors were assigned individually as a function of their concentration (e.g. Sn/cassiterite, Fe/magnetite with high concertation received relatively low errors). Depending on the assigned errors, the streams were allowed to adjust until a balanced state was reached. The objective function, giving back the sum of residuals, was minimized with the "nlm" (nonlinear minimization) package in R.

6. Acknowledgement

Chris Broadbent

(1956 to 2020)

BSc, PhD, CEng, CEnv, MAE

Publication bibliography

ALS Geochemistry (2020): Schedule of Services and Fees. EUR.

Buchmann, Markus; Schach, Edgar; Leißner, Thomas; Kern, Marius; Mütze, Thomas; Rudolph, Martin et al. (2020): Multidimensional characterization of separation processes – Part 2: Comparability of separation efficiency. In *Minerals Engineering* 150, p. 106284. DOI: 10.1016/j.mineng.2020.106284.

Buchmann, Markus; Schach, Edgar; Tolosana-Delgado, Raimon; Leißner, Thomas; Astoveza, Jennifer; Kern, Marius et al. (2018): Evaluation of Magnetic Separation Efficiency on a Cassiterite-Bearing Skarn Ore by Means of Integrative SEM-Based Image and XRF–XRD Data Analysis. In *Minerals* 8 (9), p. 390. DOI: 10.3390/min8090390.

Doebelin, Nicola; Kleeberg, Reinhard (2015): Profex: a graphical user interface for the Rietveld refinement program BGMN. In *Journal of applied crystallography* 48 (Pt 5), pp. 1573–1580. DOI: 10.1107/S1600576715014685.

Fandrich, Rolf; Gu, Ying; Burrows, Debra; Moeller, Kurt (2007): Modern SEM-based mineral liberation analysis. In *International Journal of Mineral Processing* 84 (1-4), pp. 310–320. DOI: 10.1016/j.minpro.2006.07.018.

Figueroa, German; Moeller, Kurt; Buhot, Michael; Gloy, Gerda; Haberla, David (2012): Advanced discrimination of hematite and magnetite by automated mineralogy. In : Proceedings of the 10th International Congress for Applied Mineralogy (ICAM). Springer, pp. 197–204.

Grant, D. C.; Goudie, D. J.; Voisey, C.; Shaffer, M.; Sylvester, P. (2018): Discriminating hematite and magnetite via Scanning Electron Microscope–Mineral Liberation Analyzer in the −200 mesh size fraction of iron ores. In *Applied Earth Science* 127 (1), pp. 30–37. DOI: 10.1080/03717453.2017.1422334.

Gu, Y. (2003): Automated Scanning Electron Microscope Based Mineral Liberation Analysis. An Introduction to JKMRC/FEI Mineral Liberation Analyser. In *Journal of Minerals & Materials Characterization & Engineering* 2 (1), pp. 33–41.

Heinig, T.; Bachmann, K.; Tolosana-Delgado, R.; van den Boogart, G.; Gutzmer, J. (Eds.) (2015): Monitoring gravitational and particle shape settling effects on MLA sampling preparation.

Kern, Marius; Kästner, Julian; Tolosana-Delgado, Raimon; Jeske, Tilman; Gutzmer, Jens (2019): The inherent link between ore formation and geometallurgy as documented by complex tin mineralization at the Hämmerlein deposit (Erzgebirge, Germany). In *Miner Deposita* 54 (5), pp. 683–698. DOI: 10.1007/s00126-018-0832-2.
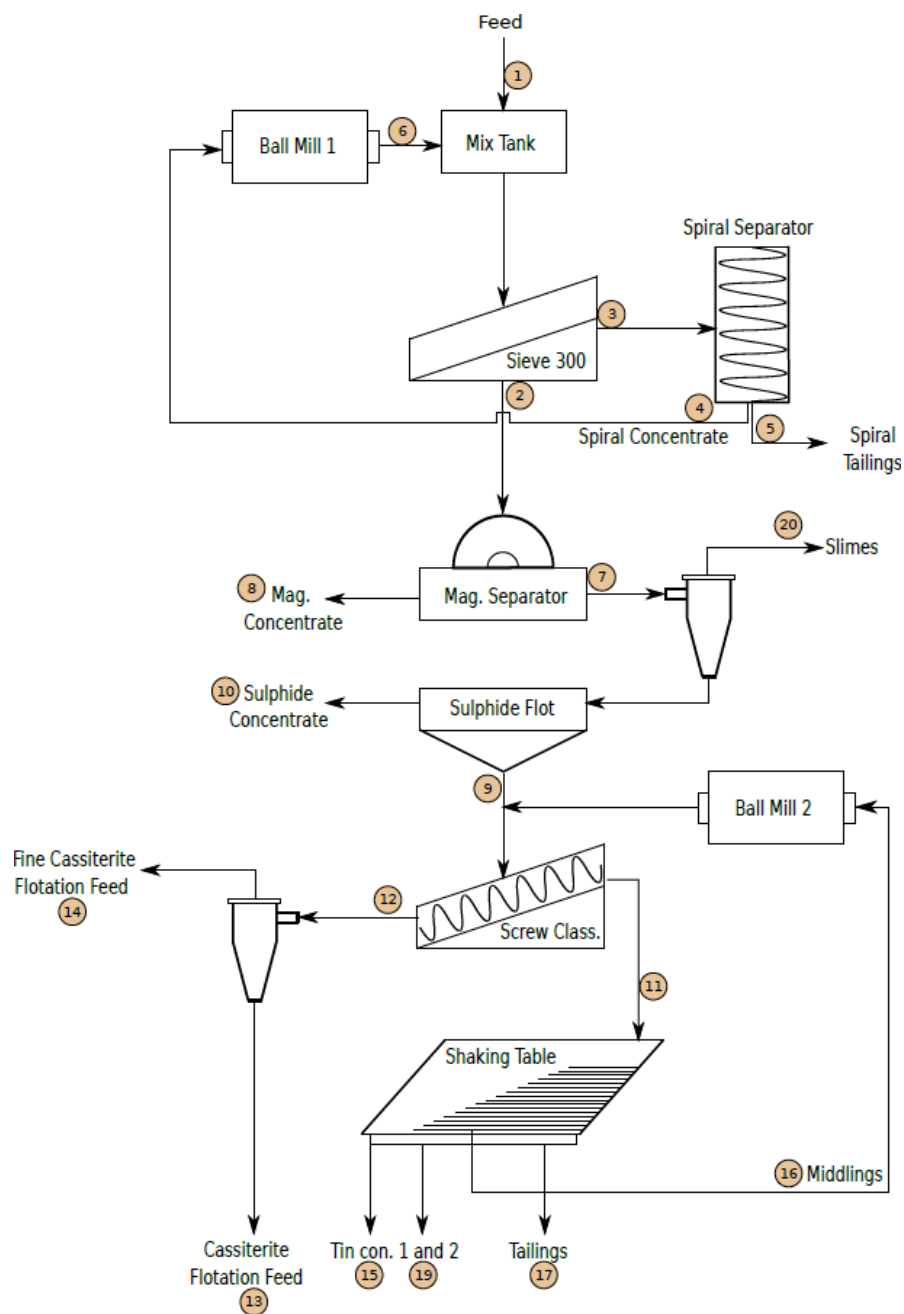
Kern, Marius; Möckel, Robert; Krause, Joachim; Teichmann, Jakob; Gutzmer, Jens (2018): Calculating the deportment of a fine-grained and compositionally complex Sn skarn with a modified approach for automated mineralogy. In *Minerals Engineering* 116, pp. 213–225. DOI: 10.1016/j.mineng.2017.06.006.

Pereira, Lucas; Frenzel, Max; Khodadadzadeh, Mahdi; Tolosana-Delgado, Raimon; Gutzmer, Jens (2020): A self-adaptive particle-tracking methodology for minerals processing. In *Journal of Cleaner Production* Under review.

Schach, Edgar; Buchmann, Markus; Tolosana-Delgado, Raimon; Leißner, Thomas; Kern, Marius; van den Boogaart, K. Gerald et al. (2019): Multidimensional characterization of separation processes – Part 1. Introducing kernel methods and entropy in the context of mineral processing using SEM-based image analysis. In *Minerals Engineering* 137, pp. 78–86. DOI: 10.1016/j.mineng.2019.03.026.

Appendix

Appendix 1: Flow sheet of the Tellerhäuser pilot plant

Appendix 2: machine list with operation parameters

Wet Sieve		Spiral Concentrator	
Manufacturer	Derrick Corporation	**Manufacturer**	Vickers Xatal
Type	Stack Sizer	**Type**	Double
Spray Water Volume (m³/h)	1.5	**Number of turns**	5
Number of decks	1	**Diameter (mm)**	600
Deck dimension (mm)	1400 x 1000	**Solid Content (kg/m³)**	~ 0.75
Sieve openning (µm)	300	**Flow Volume (m³/h)**	~ 4
Sieve material	Polyurethane		
Flow Volume (m³/h)	1.5 - 2.5		
Ball Mill 1		Ball Mill 2	
Manufacturer	SKET Magdeburg	**Manufacturer**	SKET Magdeburg
Type	Ball mill	**Type**	Ball mill
Lining	Rubber	**Lining**	Stell
Dimension (mm)	800 (L) x 500 (D)	**Dimension (mm)**	500 (L) x 500 (D)
Ball Charge (kg)	300	**Ball Charge (kg)**	110
Ball size (mm)	20 and 30	**Ball size (mm)**	18
Power (kW)	10	**Power (kW)**	4.6
Solid Content (kg/m³)	~ 2.2	**Solid Content (kg/m³)**	~ 0.8
Flow Volume (m³/h)	1.0 - 1.5	**Flow Volume (m³/h)**	~ 0.04
Magnetic Separator		Shaking Table	
Manufacturer	SKET Magdeburg	**Manufacturer**	SKET Magdeburg
Type	Wet Low Intensity	**Number of decks**	1
Model	HPMTA 900/300	**Deck Dimension (mm)**	3500 x 1500
Drum Dimension (mm)	900 (D) x 300 (W)	**Washing water (m³/h)**	1.3
Rotation Speed (rpm)	18	**Solid Content (kg/m³)**	~ 700
Drum rotation	Concurrent	**Flow Volume (m³/h)**	~ 0.3
Solid Content (kg/m³)	~ 0.2		
Flow Volume (m³/h)	~ 1.5		
Spiral Classifier		Flotation Cells	
Manufacturer	SKET Magdeburg	**Copper Sulphate (g/t)**	150-300
Type	1 screw	**Potassium Amyl Xanthate (g/**	50 - 100 g/t
Dimension (mm)	5000 x 600	**MIBC (g/t)**	25 - 75
Solid Content (kg/m³)	0.2 - 0.3	**Residence Time (min)**	20
Flow Volume (m³/h)	~ 1.5	**Solid Content (kg/m³)**	~ 0.3
		Flow Volume (m³/h)	~ 1.5
Hydrocyclone 1		Hydrocyclone 2	
Manufacturer	Mozley	**Manufacturer**	AKW
Type	SC 330	**Type**	RWS 105
Diameter (mm)	75	**Diameter (mm)**	40
Solid Content (kg/m³)	~ 0.15	**Solid Content (g/l)**	600 - 800
Flow Volume (m³/h)	~ 1.5	**Flow Volume (m³/h)**	~ 0.7